CONDITION MONITORING OF HELICOPTER GEARBOXES BY EMBEDDED SENSING[1]

Abhijit Suryavanashi, Graduate Research Assistant
Shengda Wang, Graduate Research Assistant
Robert Gao, Associate Professor
Kourosh Danai, Professor[2]
Department of Mechanical and Industrial Engineering
University of Massachusetts Amherst, Massachusetts

David G. Lewicki
Vehicle Technology Directorate
U.S. Army Research Laboratory
NASA Glenn Research Center
Cleveland, OH

ABSTRACT

Health of helicopter gearboxes is commonly assessed by monitoring the housing vibration, thus it is challenged by poor signal-to-noise ratio of the signal measured away from the source. It is hypothesized that vibration measurements from sensors placed inside the gearbox will be much clearer indicators of faults and will eliminate many of the difficulties faced by present condition monitoring systems. This paper outlines our approach to devising such a monitoring system. Several tasks have been outlined toward this objective and the strategy to address each has been described. Among the tasks are wireless sensor design, antenna design, and selection of sensor locations.

INTRODUCTION

Present helicopter power train are significant contributors to both flight safety incidents and maintenance costs. Rapid and reliable detection and diagnosis (isolation) of faults in helicopter gearboxes is therefore necessary to prevent major breakdowns due to progression of undetected faults, and for enhancing personnel safety by preventing catastrophic failures. Fault detection and diagnosis is also necessary for reducing maintenance costs by eliminating the need for routine disassembly of the gearbox, and for saving time during inspection.

Detection and diagnosis of helicopter gearbox faults, like most rotating machinery, is based upon oil analysis and vibration monitoring. Oil analysis is used to detect the presence of metallic debris by: (1) magnetic plugs (chip detectors), (2) oil filters, or (3) Spectrometric Oil Analysis (SOA) [1, 2]. Vibration monitoring is performed to detect abnormal vibration resulted from faults, with the analogy that under normal operating conditions, each component in the gearbox produces vibrations at specific frequencies which are related to the component's rotational frequency. In case of a component fault, the vibration generated by the faulty component will be different from the normal vibration, reflected at the component's rotational frequency and its harmonics. In order to be nonintrusive, vibration is measured by accelerometers mounted on the housing. But this leads to difficulty in detecting vibration changes caused by component faults, due to the attenuation of vibration by the housing and the relatively long vibration travel path between the component fault and the externally mounted accelerometers.

In order to enhance identification of changes in vibra-

[1]Presented at the American Helicopter Society 58th Annual Forum, Montreal Canada, June 11-13, 2002.

[2]To whom all correspondence should be addressed Email: danai@ecs.umass.edu

tion due to component faults, vibration analysis is performed at two levels: (1) feature extraction, and (2) data integration (fusion). At the feature extraction level, the raw vibration is processed to yield 'features' associated with the frequencies related to the gearbox components. Accordingly, considerable effort has been directed towards identification of individual features that would consistently reflect specific gearbox faults [3, 4, 5]. At the integration level, the multitude of features obtained from several accelerometers are studied together to detect the presence of an abnormality and its source. In the traditional approach to data integration, a human diagnostician first identifies abnormalities in vibration features. He/she then relates these features to component faults based on the proximity of the accelerometer producing those features as well as the type of component fault characterized by the feature. Using this information, the diagnostician hypothesizes faults in specific components and then verifies or discards the hypothesis by examining features from other accelerometers in the proximity of the suspect component. In order to facilitate the integration of vibration at this level, pattern classifiers in the form of neural networks have been proposed [6, 7, 8, 9] to take advantage of their nonlinear pattern classification capability, improved robustness to noise, and computational efficiency. Despite significant progress in feature extraction and data fusion, monitoring systems are hampered by the inherent poor signal-to-noise (S/N) ratio of the vibration measured on the housing.

The objective of this research is to explore the utility of embedded sensors in condition monitoring, to take advantage of the improved clarity attained from their close proximity to the source of signal generation. The recent advances in sensor miniaturization technology, as witnessed by the rapid development of MEMS (Micro-Electro-Mechanical Systems) [10], has led to development of advanced miniaturized sensors that have been increasingly applied to on-line condition monitoring of mechanical systems and processes [11, 12]. Compared to their conventional counterparts, the small dimension and light weight of these new sensors make it possible to place them close to the source, without causing appreciable disturbance in the dynamics of the host system. It has been shown in prior research [13] that the physical proximity of the sensors to the component faults will result in higher signal-to-noise ratios, and will naturally lead to improved signal acquisition and feature extraction.

The feasibility of embedded sensing for gearbox health monitoring is evaluated in application to an OH-58A helicopter gearbox (Fig. 1). The use of embedded wireless sensors introduces new concerns in regard to sensor placement and feature extraction. The designer now has access to a multitude of potential sensor locations within the gearbox that were previously unavailable. Moreover, some of these locations will be on rotating components with variable travel paths to individual faults. As the basis of methodical sensor location selection, a connectionist network model of the gearbox structure is proposed to represent the travel paths between potential sensor locations and component faults. The parameters of this network will be initialized according to a finite element model of the gearbox and then calibrated by structural modal experiments. The information derived from these travel paths will then be used to define an effective suite of sensor locations according to their accelerometer coverage (i.e., the number of components each location covers), and the level of redundancy between various locations [14]. Embedded sensing of gearboxes also creates new challenges such as space constraints, signal transmission difficulties, effect of rotation on the measured vibration and feature extraction, and harsh operating conditions inside the gearbox. Strategies for addressing some of these issues are also discussed in this paper.

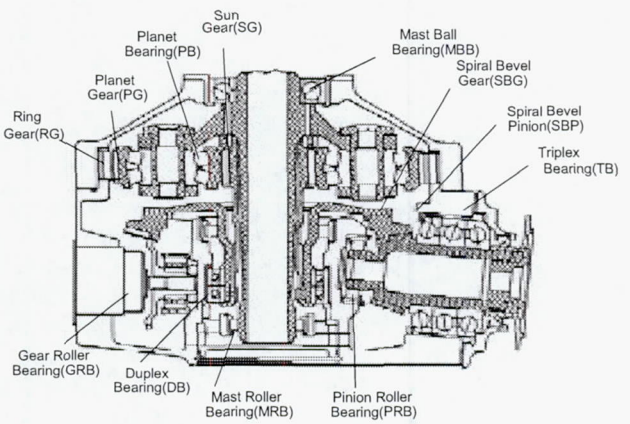

Figure 1: Layout of the various components in the OH-58A helicopter gearbox.

WIRELESS SENSING

Vibration signals measured by an embedded sensor can be transmitted wirelessly by optical and electromagnetic means. Optical means based on infrared or laser

requires line-of-sight for data transmission and reception, which is generally not available due to blockage by contamination and/or machine structure. On the other hand, electromagnetic-based radio frequency (RF) air-link is not restricted by the line-of-sight constraint, but is constrained by the shielding effect of the metallic housing. This constraint can be bypassed by inclusion of a non-metallic window on the housing and incorporation of a more elaborate antenna design.

Requirements and Constraints

The embedded sensing module will contain a sensing element, a signal processing circuit (charge amplifier), and a wireless transmitter. The RF wireless communication design will be subject to several spatial and physical constraints:

1. The wireless transmitter, together with the sensing element and measurement electronics such as the signal conditioning circuit, will be constrained to small slots, typically on the order of 18 mm × 34 mm × 4 mm [15]. The slot for the sensing module will need to be cut within each component.

2. Bandwidth of at least 10 kHz will be required to cover the spectrum of vibration typically generated in the gearbox [16].

3. The antenna length is limited to the restricted space inside and around the slot cut in the component. The electromagnetic shielding effect of the surrounding metallic structure will also need to be considered. High noise immunity is required to reduce the influence of possible environmental electro-magnetic interference on the signal. This is particularly important for early detection of faults when the fault-generated vibration is weak during the earlier stages of faults.

A circuit design that satisfies the space constraint will need to use the least number of components for the sensing module. The bandwidth specification also affects the design for wireless data transmission. Moreover, to achieve the best RF transmission efficiency, the antenna must be longer than one quarter of the carrier's wavelength l [17]. A carrier of higher frequency (f) has a shorter wavelength according to the relationship $f\lambda = c$ (where c denotes the speed of light 3×10^8 m/s), but requires more power. For this study, the frequency of 916 MHz is chosen, which is located within the license-free 902-928 MHz industrial, science and medical application (ISM) band, provided that the maximum transmitting power is less than 1W [18]. The shortest antenna length required for optimal signal radiation is calculated to be 8 cm ($\lambda/4$). To enable signal transmission, the physical size of the non-metallic housing window needs to satisfy the $\lambda/4$ requirement.

Different Modulation Schemes

Different modulation schemes can be used for transmitting analog signals. Frequency modulation (FM), amplitude modulation (AM), and digital pulse coded modulation (PCM) have been widely used in telemetry [17]. Among the three modulation schemes, AM modulation is less often used when accuracy is important, whereas PCM and FM account for about 85% of telemetry applications because of their good signal transmission quality [17]. Other modulation schemes are generally too complicated for miniaturization of sensing components within a gearbox.

The S/N ratio is an important consideration when selecting a modulation scheme for wireless transmission. For a signal transmission channel with white Gaussian noise, the S/N ratios of FM and AM modulation are defined, respectively, as [19]:

$$SNR_{\mathsf{FM}} = 3\beta^2 \frac{P_{\mathsf{m}}}{\max m^2(t)} \times \frac{P_{\mathsf{T}}}{N_0 W} \tag{1}$$

$$SNR_{\mathsf{AM}} = n \frac{P_{\mathsf{T}}}{N_0 W} \tag{2}$$

where P_{T} denotes the power of the total signal transmitted, P_{m} represents the power of the message signal $m(t)$, $n(\leq 1)$ denotes the ratio of P_{m} to P_{T}, N_0 represents the power spectral density of white Gaussian noise, W denotes the bandwidth of the message signal $m(t)$, and β represents the FM modulation index.

In the above equations, the message signal $m(t)$ is the input to the transmitter, and the term $\frac{\mathsf{P_m}}{\mathsf{max\, m^2(t)}}$ is no greater than 1 since it is the power of the normalized message signal ($\frac{\mathsf{m(t)}}{\mathsf{max\,|m(t)|}}$). The FM modulation index β is defined as the ratio of the frequency deviation to the highest frequency in the message signal. To reduce the signal distortion in FM, β is often selected such that $\beta \geq 5$ and $3\beta^2 \frac{\mathsf{P_m}}{\mathsf{max\, m^2(t)}}$ is much greater than 1 for high S/N ratio. Hence, the S/N ratio of FM is about $3\beta^2$ times higher than that of AM.

The drawback of using FM is that a wider channel bandwidth is required than in AM. For the gearbox vibration with a bandwidth of about 10 kHz, the corresponding bandwidth for AM signal transmission will

be $BW_{\mathsf{AM}} = 2f_{\mathsf{m}} = 20kHz$. The bandwidth needed for FM with $\beta = 5$ will be 120 kHz according to Carson's Rule [20]:

$$BW_{\mathsf{FM}} = 2f_{\mathsf{m}}(\beta + 1) \tag{3}$$

which is 6 times wider than required for the AM transmission bandwidth. The bandwidths needed for other digital modulation techniques, such as PCM, depend on the sampling frequency, A/D conversion resolution, and the digital transmitter. For a sampling frequency f_{s}, N-bit A/D conversion, and amplitude shift keying (ASK) modulation, the bandwidth for PCM will be $BW_{\mathsf{PCM}} = 2f_{\mathsf{s}}N$. For example, for $f_{\mathsf{s}} = 100$ kHz and $N = 12$ bits, the BW_{PCM} will be 2400 kHz, which is 20 times wider than that of FM, and 120 times that of AM. Wide bandwidths not only make the implementation of miniaturization more difficult, they will reduce channel capacity. Since noise immunity is the most critical requirement for gearbox condition monitoring, the PCM data transmission scheme is selected for its good S/N ratio transmission, but its circuitry is simplified using a voltage-to-frequency (VFC) scheme.

Transmitter Design

The schematic of the designed PCM transmitter is shown in Fig. 2. It includes an A/D converter, a parallel-to-serial converter, and a RS232 encoder for data packaging and synchronization that may require coordination by a microprocessor. The advantage of PCM is that in conjunction with A/D converter the data format of receiver output is ready for a microprocessor or a computer, and digitization error can be neglected.

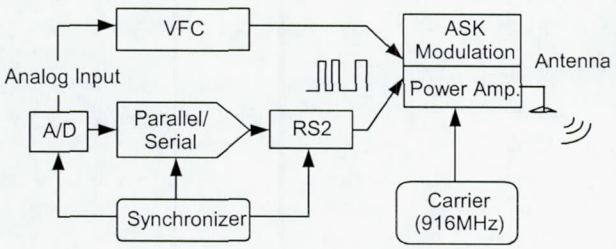

Figure 2: Schematic view of the data transmitter.

In miniaturization of the sensing module, in addition to the single chip design to satisfy the size requirement, the input and output signal dynamic range, single power supply, power consumption, and IC die availability need to be considered for the VFC design. A monolithic digital ASK transmitter TX6000 [21] is selected to transmit the frequency modulated (FM) signal from VFC. Hence, the VFC frequency output has to match the input throughput capacity of TX6000, i.e., a nominal data rate of 115.2 kbps. For a square wave, the high and low voltage levels represent different binary bits, and since one single-cycle square wave represents two bits of data, the 115.2 kbps data rate sets the upper frequency limit of the square wave from the VFC to 57.6 kHz. This is implemented by a VFC chip LM331 that outputs square waves of 56.5 kHz. Under the control of the conditioning circuit output, the VFC output contains the frequency range of 26.4 kHz to 55.4 kHz and has a non-linearity of about 0.13%. It can be shown that using the VFC design with an output frequency range 26.4 - 55.4 kHz and the TX6000 transmitter, a bearing signal with the maximum frequency of up to 2 kHz can be transmitted with 98% of the signal energy retained, resulting in a signal distortion ratio of 2% [20]. The physical size of the developed circuit can be reduced by using the surface mount (SMT) and hybrid techniques, as shown in Fig. 3.

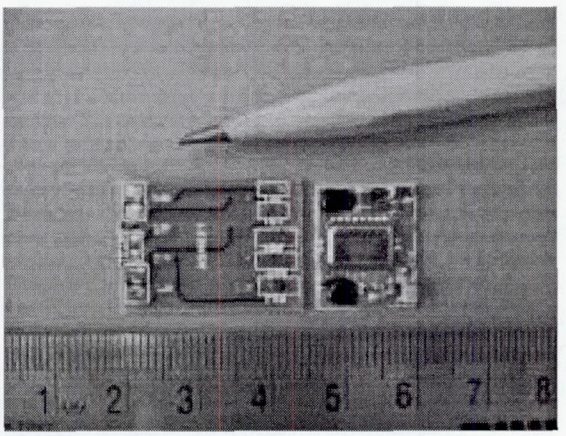

Figure 3: Prototype of the RF transmitter using hybrid techniques.

The signal sensing and transmission capability of the designed wireless sensor module, incorporating the RF transmitter and a piezoceramic sensing element, was compared with that of a standard Kistler accelerometer (model # 8692B50). The wireless sensor was mounted in a back-to-back arrangement on the Kistler sensor, which was mounted on the ring gear of the planetary subsystem of the OH-58A helicopter gearbox. The top case was then replaced and bolted down. The wired connection for the Kistler sensor was routed

through an opening in the top case which is reserved for the output shaft of the gearbox. The same opening also allowed the signal to be transmitted wirelessly outside the gearbox. In the final design, it is envisioned that an opening in the casing sealed by a plastic cap (similar to an oil level indicator) will serve as the pathway for the wireless signal. An impulse was introduced onto the outer casing by an impact hammer and signals from both sensors were recorded. The power spectral density (PSD) plots of the signals measured by the two sensors, along with their correlation, are shown in Fig. 4. The results indicate that the cross-correlation between the Kistler sensor signal and the wireless signal have a maximum value at zero phase lag. The variation around the maximum value is due to the noise present in the two signals. The characteristic high correlation coefficient at zero phase lag and the sharp drop for even small phase differences indicate that the wireless sensor functions as the commercial sensor.

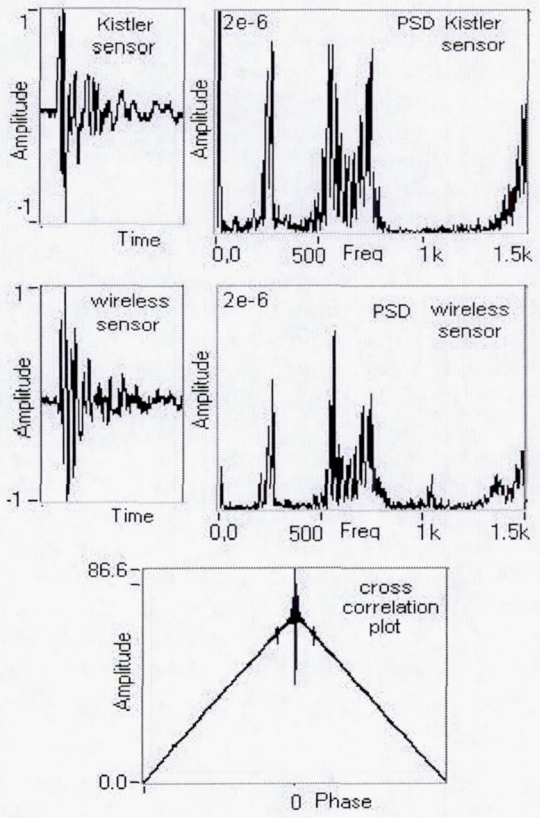

Figure 4: *Frequency spectral density of the signals measured by the two sensors and their correlation.*

SENSOR LOCATION SELECTION

Sensor placement is an important consideration in embedded sensing, since a balance needs to be provided between the number of sensors used and the coverage of the possible faults within the various components. To illustrate this concept, one may consider the coverage of faults on the ring gear, the planet gear, and the sun gear by a sensor mounted on a planet of the OH-58A gearbox (Fig. 5). The transmission of vibration to the sensor from the three faults varies as the gears mesh with one another at the fault locations. For Fault 1, there will be two sources of excitation: one when the planet meshes with the ring gear and the other when the planet meshes with the sun gear. For both sources, however, the travel paths are approximately the same. For Fault 2, where the fault is on a planet gear different from the one with the sensor, there will be the same two sources of excitation, but the travel paths will differ – one path includes the ring gear while the other includes the sun gear. For Fault 3, the vibration measured by the sensor will be the weakest when the other planets come into contact with the ring gear at the fault location, until the sensor-mounted planet itself meshes the ring gear at the fault location.

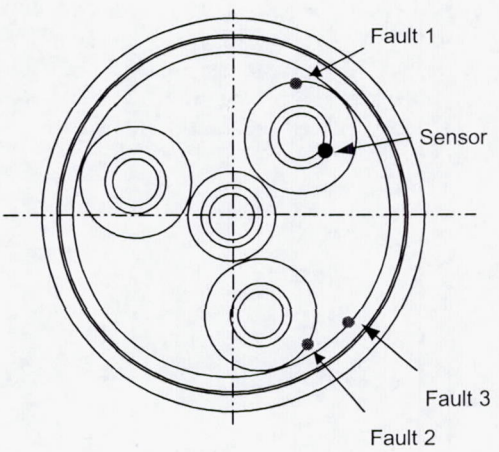

Figure 5: A possible sensor placement scenario

As illustrated in the above example, sensor placement needs to be performed by considering the travel paths between various faults and the candidate locations. Methodical specification of such travel paths may be

performed through a connectionist network representation of the gearbox structure. A network representation of the OH-58A helicopter main gearbox is shown in Fig. 6, where the nodes represent the individual components of the gearbox (1 - Top Case; 2 - Ring Gear; 3 - Planet Gear 1; 4 - Planet Gear 2; 5 - Planet Gear 3; 6 - Spider ; 7 - Sun Gear; 8 - Output Shaft; 9 - Main Input Gear Shaft; 10 - Casing; 11 - Bevel Gear; 12 - Main Case; 13- Bevel Pinion; 14 - Input Shaft) and the connections denote the interface points between the components. This diagram identifies the dominant travel paths present in the gearbox. In this diagram, the interfaces between component pairs are represented by impedance values, to define the attenuation of vibration at each interface, and the nodes represent the effective mass of individual components, as well as the potential sensor locations. The impedance values can be estimated crudely through lumped mass modeling of the gearbox components or by finite element analysis. In lumped mass modeling, the interface comprises a spring element, that accounts for the stiffness of gear meshes and bearings, and a damper, which represents the damping due to the component material. Since bearings are assumed not to be used for sensor placement, they are considered only as interfaces. Desirable sensor locations are those with the widest reach.

To preserve its simplicity, several assumptions are made in defining the proposed network: (a) the average stiffness of a gear mesh is taken into account, instead of the variable stiffness from the varying roll angle of the gear pair, (b) vibration in only one direction is considered, (c) only dominant transmission paths are considered, and (d) effects of lubrication, friction and backlash are neglected. In the above network, the components are denoted by $v_i \in V$ and contact points by $e_j \in E$. As such, an excitation at a component, say v_1, will have the propagation path $v_1 - v_2 - v_3$ to reach a sensor placed on component v_3.

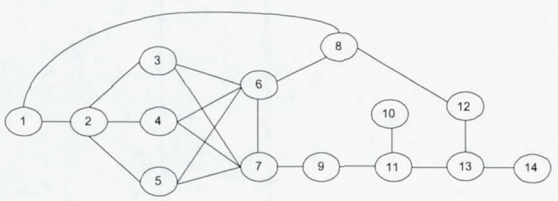

Figure 6: Network representation of gearbox structure.

During the propagation of vibration, some energy is lost due to elasticity and damping in the path. To represent such energy loss, the signal pass ratio for contact interface between v_i and v_j can be defined as

$$w_{ij} = \begin{cases} log(\psi_j{}^2/\psi_i{}^2) & \text{if } e_{ij} \in E \\ 0 & otherwise \end{cases} \quad (4)$$

where ψ_j^2 and ψ_i^2 are the Mean Square Values of the signals at component v_j and v_i, respectively.

For a path $v_i - v_{i+1}, \cdots, v_j$, in order to represent the signal attenuation through the path, the weighted distance of the path is defined as the signal pass ratio of the path:

$$dw_{ij} = log(\psi_j{}^2/\psi_i{}^2) = \sum_{k=i}^{j-1} w_{k,k+1} \quad (5)$$

According to the above terminology, the sensor location selection problem can be defined as follows. Given the network representation of the gearbox $G(V, E)$, a subset of components $V_o \in V$ needs to be found such that:

1. For each component $v_i \in V$ in the network, there exists a component $v_j \in V_o$ such that there is a path from v_i to v_j whose weighted distance $dw_{ij} > dw_0$, where dw_0 is a threshold.
2. the size of Vo, $|Vo|$, is minimized.

The network representation of the gearbox structure provides a convenient means of addressing sensor location selection, in addition to its apparent utility for fault diagnosis. As mentioned earlier, the parameters (weights) of this network will be defined as the impedance values (attenuation gains) of each component. For their initial values, these parameters can be defined according to a finite element model of the gearbox (Fig. 7), and then calibrated according to experimental modal analysis of the gearbox. The devise of an efficient calibration routine that can tune the network parameters with a limited number of experimental data is a major focus of this research.

As a validation exercise for network calibration, experiments were conducted to determine the magnitude of vibration responses at five representative sensor locations inside and outside of the gearbox. The experimental setup is shown in Fig. 8, where fault-induced vibration at each location is simulated by impulse hammer strikes. The hammer has a built-in

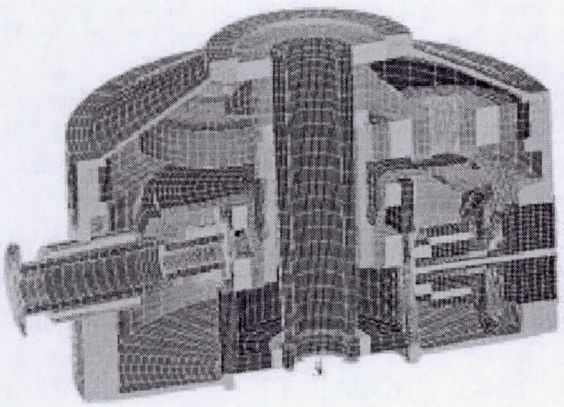

Figure 7: Finite element model of the OH-58A Gearbox.

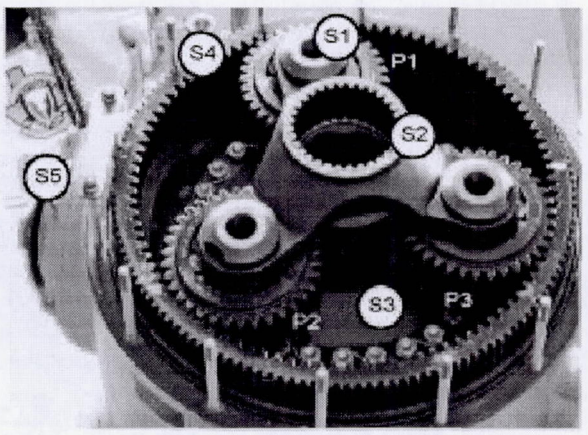

Figure 8: Experimental setup for the sensor placement sensitivity.

acceleration sensor that captures the impulse. Five Kistler accelerometers (model # 8630A5, # 8636B50 and # 8692B50) were used to measure vibration intensity at the five locations. A sample of sensitivity values obtained from the experiments are shown in Table 1, indicating the individual responses of sensors to force impulses applied at potential fault locations. The sensitivity values were computed as the ratio of the rms values Ψ of the signals, as

$$SM_{ij} = \frac{1}{6} \sum_{k} \frac{\Psi_{ij}^{sensor}(k)}{\Psi_{i}^{excitation}(k)} \qquad (6)$$

where k denotes the number of sample data signals taken for each fault-sensor combination ($k = 6$, in this case), $i =' a', \cdots, 'g'$ represents the fault location, and $j = S1, \cdots, S5$ denotes the sensor location. The sensor locations, as indicated in Fig. 8, were: S1: Planet Shaft (P1 is the planet on which S1 was mounted), S2: Spider, S3: Main Input Gear Shaft, S4: Planetary Ring Gear, and S5: Main Input Pinion Adapter. The fault locations were: (a) fault on Ring Gear (Ring Gear-P1 mesh), (b) fault on P1 (Ring Gear-P1 mesh), (c) fault on P2 (Ring Gear-P2 mesh), (d) fault on Sun Gear (Sun Gear-P1 mesh), (e) fault on P1 (Sun Gear-P1 mesh), (f) fault on Input Bevel Gear (Input Gear-Pinion mesh), and (g) fault on Input Pinion (Input Gear-Pinion mesh). For each fault location, the values were then normalized with respect to the maximum coefficient in each row. The sensitivity values such as the ones presented in Table 1 will be the basis for calibrating the network model of the gearbox.

Table 1: Experimentally obtained sensitivity values between the sensor and fault locations.

Excitaion Location	Sensor Location				
	S1	S2	S3	S4	S5
a	0.014	0.015	0.055	1.000	0.222
b	1.000	0.533	0.124	0.205	0.132
c	0.621	1.000	0.158	0.125	0.125
d	0.367	1.000	0.281	0.290	0.711
e	1.000	0.497	0.148	0.208	0.134
f	0.007	0.012	1.000	0.039	0.029
g	0.022	0.015	0.074	0.210	1.000

FUTURE WORK

Future work in this research will focus on all aspects of the topics discussed above. Specifically, it will include:

1. The Network Model. As mentioned earlier, the parameters of the network model will need to be defined and then calibrated according to experimental data. The strategy for calibrating the network will incorporate theoretical, experimental, and finite element analysis. The network will be initialized by simulated vibration from a finite element model of the gearbox, and then refined according to experimental interface-activated energy transfer to various sensor locations. The fine-tuned network will then be used as the basis for sensor selection and fault diagnosis. It should be noted that the current network represents vi-

bration transfer in only one direction. As such, three parameter values will need to be defined for each connection or node to cover energy transfer in x, y and z directions.

2. Sensor Location Selection. The network model will provide a systematic means of defining the attenuation of vibration between component interfaces and potential sensor locations. A sensor location selection strategy will be formulated next to use the information from the network to estimate the coverage and overlap of each location as the basis for sensor location selection.

3. Sensor Design. The sensor used for the current feasibility study has a limited bandwidth suitable for bearing fault detection. For gearbox fault detection, a sensor with a bandwidth of 20 kHz will be designed. Since this sensor will be exposed to a harsh environment and inertial forces typical of rotating components, issues related to sensor packaging and testing will need to be addressed as well. With the best sensor locations identified, experiments will be conducted to determine the best ways to access the signal wirelessly outside the gearbox with minimum modifications to the existing housing. This will also involve addressing antenna design issues within a maximally shielded environment.

4. Signal Processing. A wireless sensor mounted on a rotating component has a variable travel path to the fault, so the signal it captures will be different from those obtained by stationary sensors. This difference may demand new signal processing algorithms and/or diagnostic reasoning techniques.

References

[1] Lurton, E. H., 1994, "Navy Oil Analysis Program Overview", Proc. JOAP International Condition Monitoring Conference, pp. 4-6.

[2] Thornton, M. G., 1994, "Filter Debris Analysis, A Viable Alternative to Existing Spectrometric Oil Analysis Techniques", Proc. JOAP International Condition Monitoring Conference, pp. 108-119.

[3] Zakrajsek, J. J., Hanschuh, R. F., Lewicki, D. G., and Decker, H. J., 1995, "Detecting Gear Tooth Fracture in a High Contact Ratio Face Gear Mesh", Proc. of 49th Meeting of the Society of Machinery Failure Prevention Technology, April, pp. 91-102.

[4] Mertaugh, L. J., 1986, "Evaluation of Vibration Analysis Techniques for the Detection of Gear and Bearing Faults in Helicopter Gearboxes", Proc. of the Mechanical Failure Prevention Group 41th Meeting, October, pp. 28-30.

[5] McFadden, P. D., and Smith, J. D., 1986, "Effect of Transmission Path on Measured Gear Vibration", Journal of Vibration, Acoustics, Stress, Reliability in Design, Vol. 108, July, pp. 377-378.

[6] Kazlas, P. T., Monsen, P. T., and LeBlanc, M. J., 1993, "Neural Network-Based Helicopter Gearbox Health Monitoring System", presented at IEEE-SP Workshop on Neural Networks for Signal Processing, Linthicum, MD, September.

[7] Chin, H., Danai, K., and Lewicki, D. G., 1993, "Pattern Classifier for Fault Diagnosis of Helicopter Gearboxes", IFAC J. of Control Eng. Practice, Vol. 1, No. 5, pp. 771-778.

[8] Solorzano, M. R., Ishii, D. K., Nickolaisen, N. R., and Huang, W. Y., 1991, "Detection and Classification of Faults from Helicopter Vibration Data Using Recently Developed Signal Processing and Neural Network Techniques", Code 535, Advanced Technology Development Branch, Naval Ocean Systems Center, San Diego, CA 92152-5000.

[9] Jammu, V. B., Danai, K., and Lewicki, D. G., 1998, "Structure-Based Connectionist Network for Fault Diagnosis of Helicopter Gearboxes," ASME J. of Mechanical Design, Vol. 120, No. 1, pp. 100-112.

[10] Moore, D. and Syms, R., 1999, "Recent Developments in Micromachined Silicon", Journal of Electronics and Communication Engineering, Vol. 11, No. 6, pp. 261-270.

[11] Varadan, V. and Varadan, V., 1999, "Microsensors and MEMS for Health Monitoring of Composite and Aircraft Structures in Flight", Proc. of SPIE Smart Structures and Materials Conference, Newport Beach, CA, Vol. 3673, pp. 359-368.

[12] Hirona, T., Fan, L., Gao, J., and Lee, W., 1998, "MEMS milliactuator for Hard-Disk-Drive Tracking Servo", IEEE/ASME Journal of Microelectromechanical Systems, Vol. 7, No. 2, pp. 149-155.

[13] Wang, C. and Gao, R. "Sensor Placement Strategy for In-Situ Bearing Defect Detection," IEEE Instrumentation and Measurement Technology Conference, Baltimore, Maryland, May 1-4, pp. 1463-1467.

[14] Wang, K., Yang, D., Danai, K., and Lewicki, D. G., 1999, "Model-Based Selection of Accelerometer Locations for Helicopter Gearbox Monitoring," J. of American Helicopter Society, Vol. 44, No. 4, pp. 269-275.

[15] Holm-Hansen B. and Gao, R., 2000, "Vibration Analysis of a Sensor-Integrated Ball Bearing," ASME

Journal of Vibration and Acoustics, Vol. 122, pp. 384-392.

[16] Lewicki, D. G., Decker, H. J., and Shimski, J. T., 1992, "Full-Scale Transmission Testing to Evaluate Advanced Lubricants", Technical Report, NASA TM-105668, AVSCOM TR-91-C-035.

[17] Stock, O., 1987, Introduction to Telemetry, Instrument Society of America.

[18] Pozar, D., 1998, Microwave Engineering, 2nd Edition, John Wiley & Sons, New York, New York.

[19] Gibson, J., 1993, Principle of Digital and Analog Communication, 2nd Edition, Prentice-Hall, New Jersey.

[20] Ziemer, R. and Tranter, W., 1985, Principle of Communications, 2nd Edition, Houghton Mifflin, Boston.

[21] RF Monolithic, 2000, "Data Sheet of TX6000 and RX6000," USA.